Phonon Limited Performance of III-V Nanowire Transistors

M.J. Gilbert[1,2] and D.K. Ferry[1]

[1]*Department of Electrical Engineering and Center for Solid State Electronics Research, Arizona State University, Tempe, AZ 85287-5706*

[2]*Microelectronics Research Center, University of Texas at Austin, Austin, TX 78758*

mgilbert@mer.utexas.edu

Abstract. We use a fully self-consistent three-dimensional quantum mechanical transport formalism to examine the performance of InAs based quantum wire transistors both in the ballistic limit and with phonon scattering included. We present a method for the inclusion of polar optical phonon scattering as a real-space self-energy term. We find that the ballistic performance of the devices can be recovered if the dopants in the system are kept away from the channel entrance and exit. When dopants are present at these key points, we find that the altered carrier energy, particularly in the source, has a significant impact on the device. This ballistic recovery is aided by the fact that at higher energies, polar optical phonon scattering loses its non-locality which leads to a reduced scattering rate in these confined systems.

1. Introduction

It has been a well established fact that the semiconductor industry is aggressively seeking alternative device solutions in order to continue the relentless scaling of device density. One of the most promising of these new technologies is the tri-gate quantum wire MOSFET (Metal Oxide Semiconductor Field Effect Transistor). Tri-gate devices offer greatly improved electrostatic control over the channel of the device when compared to the traditional MOSFET due to the presence of the additional gates [1].

Within the last few years, there has been a renewed interest in the use of III-V materials instead of silicon for future generation transistors [2]. Previous studies have shown that care must be taken in the fabrication of these devices or large increases in the output drain current (kink effect) occur [3-4]. However, it has been shown that through the use of quantum wires with discrete subbands for the active regions of the device, the kink effect may be eliminated.

In this paper, we present the results of a three-dimensional, self-consistent, quantum mechanical device simulation of several tri-gate InAs quantum wire MOSFETs. Here we present results of 10 nm channel length devices both in the ballistic limit and with the effects of impurity, acoustic deformation potential, intervalley ($\Gamma \rightarrow X$ and $\Gamma \rightarrow L$) and, polar optical phonon (POP) scattering as separable real space self-energy terms.

2. Device Structure

In fig. 1, we display a schematic of the device geometry for an InAs MOSFET with a 9.69 nm channel taken to lie in the *x-y* plane (the *z*-axis is normal to the plane shown). The exact device dimensions (multiples of the lattice constant) have been included in this simulation to aid in the inclusion of the discrete dopants. The thickness of the InAs layer is 9.09 nm. The source and drain of the device are *n*-type with a doping density of 6×10^{18} cm^{-3}, while the channel of the device is considered to be *p*-type, but left undoped. The gate material is assumed to be platinum and the gate oxide on each side is composed of 1 nm of hafnium oxide (HfO$_2$). Underneath the device, we have assumed a generic insulating substrate. Once the device geometry is defined, the InAs lattice is scanned and the dopants are distributed according to the method presented in [5]. Following the distribution of the dopants, they are then mapped back onto the grid of the simulation mesh and the initial self-consistent Poisson solution is obtained. In this case, the full Coulomb potential of the dopants is incorporated. Then, the solution of Poisson's equation for the local potential is no longer smoothly varying in the source and

1. REPORT DATE **2006**	2. REPORT TYPE **N/A**	3. DATES COVERED **-**	
4. TITLE AND SUBTITLE **Phonon Limited Performance of III-V Nanowire Transistors**		5a. CONTRACT NUMBER	
		5b. GRANT NUMBER	
		5c. PROGRAM ELEMENT NUMBER	
6. AUTHOR(S)		5d. PROJECT NUMBER	
		5e. TASK NUMBER	
		5f. WORK UNIT NUMBER	
7. PERFORMING ORGANIZATION NAME(S) AND ADDRESS(ES) **Department of Electrical Engineering and Center for Solid State Electronics Research, Arizona State University, Tempe, AZ 85287-5706**		8. PERFORMING ORGANIZATION REPORT NUMBER	
9. SPONSORING/MONITORING AGENCY NAME(S) AND ADDRESS(ES)		10. SPONSOR/MONITOR'S ACRONYM(S)	
		11. SPONSOR/MONITOR'S REPORT NUMBER(S)	
12. DISTRIBUTION/AVAILABILITY STATEMENT **Approved for public release, distribution unlimited**			
13. SUPPLEMENTARY NOTES **The Seventh International Conference on New Phenomena in Mesoscopic Structures & The Fifth International Conference on Surfaces and Interfaces of Mesoscopic Devices, November 27th - December 2nd, 2005, Maui, Hawaii, USA**			
14. ABSTRACT			
15. SUBJECT TERMS			

16. SECURITY CLASSIFICATION OF:			17. LIMITATION OF ABSTRACT **SAR**	18. NUMBER OF PAGES **6**	19a. NAME OF RESPONSIBLE PERSON
a. REPORT **unclassified**	b. ABSTRACT **unclassified**	c. THIS PAGE **unclassified**			

the drain of the device. The inclusion of discrete dopants causes the formation of potential variation in the source and drain. The density throughout the device is calculated using a variant of the recursive scattering matrix method which solves the Schrödinger equation in the effective mass approximation as described in [6]. In short, this method provides us with a three-dimensional, fully quantum mechanical method. Since the transport calculation is performed in real space, the different excited modes in the system are automatically coupled unlike in other simulations [7]. In order to achieve self-consistency, the density obtained from the transport calculation is then updated using Broyden's method [8] and a new guess for the potential is obtained through the solution of Poisson's equation. The process is repeated until a desired level of convergence is obtained. It should be noted that all of the simulations presented here have been performed at 300 K.
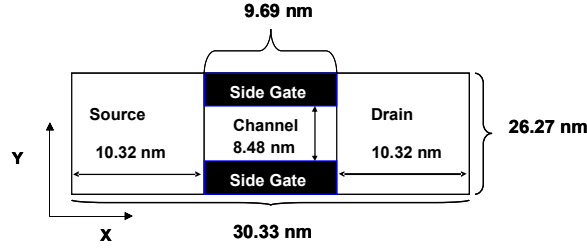

Figure 1: Schematic of the device under consideration taken in the *xy* plane.

3. Polar Optical Phonon Scattering

The inclusion of separable scattering mechanisms is not a new concept. In previous work, acoustic and optical phonon processes have been derived [9] and so the work will not be repeated here. However, we are now interested in including polar optical phonons which, to this point, have not been treated. We begin by noting that to use the method presented in ref. 9, we are assuming that the scattering is weak relative to the energies in the system, and that we are only interested in the steady state limit. Therefore, we can use the Fermi golden rule expression, equivalent to a first-order, non-self-consistent Born approximation, for each of the scattering processes and generate a real space self-energy from it. In particular, we note that the imaginary part of the self-energy term is related to the scattering rate and it is the latter scattering rate that we wish to calculate [9]. This will result in an *x* directed momentum which is related to the carrier energy in the quantum wire. Since many of the details of the derivation of similar scattering rates are outlined in ref. 9, we will show only the important changes in the derivation. In this paper, we use the Fermi golden rule for scattering. This is treated in many other places and the only modification that we need is to account for the transverse modes of the quantum wire. Therefore, we begin with the general form

$$\left(\frac{1}{\tau_{polar}}\right)_{nm}^{n'm'} = \frac{\pi e^2}{\gamma V \omega_0} \sum_{q_x} \sum_{q_y, q_z} \int dy \int dz \int dy' \int dz' \varphi_{i,j}^*(y,z) \varphi_{i',j'}(y,z) \varphi_{i,j}^*(y',z') \varphi_{i',j'}(y',z')$$
$$\frac{e^{iq_y(y-y')+iq_z(z-z')}}{q^2} \left\{ (N_q+1)\delta(E_k - E_{k-q} - \hbar\omega_0) + N_q \delta(E_k - E_{k-q} + \hbar\omega_0) \right\} \qquad (1)$$

The delta functions in eq. (1) serve to conserve the energy in the process of the interactions of the carriers with the polar optical phonons. $\varphi_{i,j}(y,z)$ is the transverse two-dimensional wave function in the particular slice under consideration. We assume in this treatment that we are dealing with parabolic bandstructure. Taking a closer look at the terms contained within the delta functions, we realize that based on this assumption

$$E_k - E_{k \pm q} \pm \hbar\omega_0 = E_{i,j} - E_{i',j'} \pm \hbar\omega_0 + \frac{\hbar^2 k_x^2}{2m_x^*} - \frac{\hbar^2 (k_x \pm q_x)^2}{2m_x^*}$$
$$= E_{i,j} - E_{i',j'} \pm \hbar\omega_0 \mp \frac{\hbar^2 k_x q_x}{m_x^*} \mp \frac{\hbar^2 q_x^2}{2m_x^*} \tag{2}$$

In eq. (2), $E_{i,j}$ and $E_{i',j'}$ are the initial and final energies at the bottom of their respective bands. We begin to simplify eq. (1), by first examining the longitudinal terms

$$\sum_{q_x} \frac{1}{2q^2} \delta\left(E_k - E_{k \pm q} \pm \hbar\omega_0\right). \tag{3}$$

We now expand eq. (3) using the results from eq. (2),

$$\sum_{q_x} \frac{1}{q_x^2 + q_y^2 + q_z^2} \delta\left(\mp \frac{\hbar^2 q_x^2}{2m_x^*} \mp \frac{\hbar^2 k_x q_x}{m} + E_{i,j} - E_{i',j'} \pm \hbar\omega_0\right) \tag{4}$$

This sum may be simplified further by taking the Fourier transform,

$$\frac{1}{2\pi} \int_{-\infty}^{\infty} \frac{e^{iq_x(x-x')}}{q_x^2 + q_y^2 + q_z^2} \delta\left(\mp \frac{\hbar^2 q_x^2}{2m_x^*} \mp \frac{\hbar^2 k_x q_x}{m} + \Delta_{i,j}^{i',j'}\right) dq_x , \tag{5}$$

where denote

$$\Delta_{i,j}^{i',j'} = E_{i,j} - E_{i',j'} \pm \hbar\omega_0 . \tag{6}$$

Representing eq. (5) as a summation, we have

$$\frac{1}{2\pi} \sum_i \frac{e^{iq_x(x-x')}}{q_{xi}^2 + q_y^2 + q_z^2} \frac{1}{\left|\partial E_{k \pm q} / \partial q_x\right|}$$
$$\frac{m_x^*}{2\pi\hbar^2} \sum_i \frac{e^{iq_x(x-x')}}{q_{xi}^2 + q_y^2 + q_z^2} \frac{1}{\left|\mp k_x + \frac{q_{xi}}{2}\right|} . \tag{7}$$

At this point we examine the relationship for $E_{k \pm q}$

$$E_{k \pm q} = \frac{\hbar^2 k_x^2}{2m_x^*} \pm \frac{\hbar^2 k_x q_x}{m_x^*} + \frac{\hbar^2 q_x^2}{2m_x^*} \tag{8}$$

Eq. (8) is quadratic in q_x and may then be solved to yield a solution for q_x which is then substituted back into eq. (7) making the term in the absolute value independent of q_x as shown below regardless if the phonon process under consideration is emission or absorption. Therefore, we may group all of the variables that are independent of q_x into a simple dummy variable a. With this pairing, we may reduce our summation in eq. (7) to reach

$$\frac{m_x^*}{2\pi\hbar^2} \sum_i \frac{e^{iq_x(x-x')}}{q_{xi}^2 + a^2} . \tag{9}$$

Eq. (9) is most easily evaluated by making a transformation to cylindrical coordinates to obtain

$$\frac{m_x^*}{4\pi^2\hbar^2} \iint \frac{q_x e^{iq_x\left(\vec{r_x} - \vec{r_x'}\right)}}{q_x^2 + a^2} d\theta dq . \tag{10}$$

We evaluate the integral in eq. (10) using contour integrations to arrive at a final, simplified expression for the sum over the longitudinal wavevectors

$$\sum_{q_x} \frac{1}{2q_x} \delta\left(E_k\right). \tag{11}$$

The expression in eq. (11) is substituted back into eq. (1) to find an overlap integral that is similar to both the one found in ref. 9 and in most textbooks

$$
\begin{aligned}
&= \sum_{q_x} \sum_{q_y, q_z} \int dy \int dz \int dy' \int dz' \varphi^*_{i,j}(y,z) \varphi_{i',j'}(y,z) \varphi^*_{i,j}(y',z') \varphi_{i',j'}(y',z') \\
&\qquad \frac{e^{iq_y(y-y')+iq_z(z-z')}}{2q_x} \delta(E_k) \\
&= \frac{A}{2V} \sum_{q_x} \iint dz\,dy \left[\varphi^*_{i,j}(y,z) \varphi_{i',j'}(y,z) \right]^2 \frac{1}{q_x} \delta(E_k) \\
&= \frac{A}{4\pi V} \sum_{k_x} I^{i',j'}_{i,j} \frac{1}{k_x} \delta(E_k)
\end{aligned}
\qquad (12)
$$

Where in eq. (12) we have used the following definition,

$$
I^{i',j'}_{i,j} = \frac{A}{4\pi^2 V} \iint dy\,dz \left[\varphi^*_{i,j}(y,z) \varphi_{i',j'}(y,z) \right]^2 . \qquad (13)
$$

Following the usual procedure, we replace the summation over the final momentum states with an integration

$$
\sum_{k'} \to \frac{L}{2\pi} \int_{-\infty}^{\infty} dk' = \int_0^{\infty} \rho_{1D}(E')dE' \qquad (14)
$$

to obtain the final result

$$
\left(\frac{1}{\tau_{polar}} \right)^{i',j'}_{i,j} = \frac{m^*_x L e^2}{32\pi^3 \gamma \omega_0} I^{i',j'}_{i,j} \int \frac{dk_x}{k_x} \delta(E_k) . \qquad (15)
$$

However, we are still in the mode space representation and the longitudinal momentum is not yet a viable operator. To remedy this, we take the inverse transform. This essentially involves solving a contour integral for both the emission and absorption cases which results from eq. (15). This gives us our final, simplified and summarized results for absorption and emission of POPs,

$$
\left(\frac{1}{\tau_{polar}} \right)^{i',j'}_{i,j} = \frac{m^*_x L e^2}{32\pi^3 \gamma \omega_0} I^{i',j'}_{i,j} \begin{cases} N_q e^{-k_0|x-x'|} \\ (N_q+1) \dfrac{\sin(k_0|x-x'|)}{k_0|x-x'|} \end{cases} . \qquad (16)
$$

This is a rather expected result as we now see the manifestation of the non-local nature of POP scattering as we see a clear dependence on the grid in eq. (16). To utilize this in the transport calculation, we must use the following unitary transformation to convert this form to the site representation for inclusion in the Hamiltonian,

$$
\Gamma_{polar} = \mathrm{Im}\{\Sigma\} = U^+ \left(\frac{\hbar}{\tau_{polar}} \right)^{i',j'}_{i,j} U , \qquad (17)
$$

where U is a unitary mode-to-site transformation matrix. The unitary matrix U^+ results from the eigenvalue solutions in the transverse slice and are composed of the various eigenfunctions in the site basis. Hence, it represents a mode-to-slice transformation.

4. Results

In fig. 2 we plot the I_d-V_g curves for the ballistic and quasi-ballistic case for two different dopant distributions. In fig. 2(a) we can clearly see that the inclusion of the phonon processes has a profound effect on the device performance. This degradation in performance can be directly linked to the inclusion of the POP scattering. The intervalley transitions ($\Gamma{\to}X$ and $\Gamma{\to}L$) are quite limited, in our case, as these satellite valleys are offset by 0.73 eV and 1.02 eV respectively. Therefore, only at high

voltages would the carriers be capable of reaching these valleys. Interactions with the acoustic phonons are still present, but never quite reach large enough energies to effect the transport in a significant manner. While it is rather expected that POP scattering causes significant reductions in device performance, the role that quantum interference appears to have in device operation is unexpected. In fig. 2(b), we plot the I_d-V_g curves for the ballistic and quasi-ballistic case for a different dopant distribution. Here we find that the device nearly recovers its ballistic device performance. This ballistic recovery is attributed to two factors, localization of the polar optical scattering process and differences in dopant locations. As the energies present in the system increase, we find that the POP scattering becomes relatively localized which leads to reductions in both the absorptive and emissive coupling. Therefore, higher energy modes are subjected to reduced scattering. Perhaps more interestingly, we find that quantum interference, of the carriers with the dopants, is not quenched in the presence of scattering. The device in fig. 2(a) has dopants present close to the source-channel and channel-drain areas which significantly impacts carrier energies of the electrons entering the channel. The device in fig. 2(b) does not have dopants near the channel entrance and exit areas, and therefore, has reduced quantum interference effects.
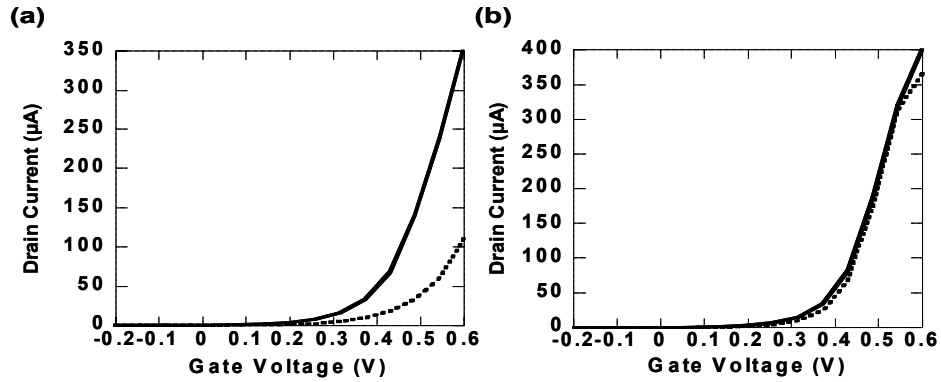
(a)   **(b)**

Figure 2: I_d-V_g curves under ballistic (solid) and quasi-ballistic (dotted) conditions for an identical dopant distribution where (a) dopants are present close to the channel interfaces, and (b) dopants are removed from the channel interface, respectively.

5. Results

In this paper, we have presented results of self-consistent three-dimensional fully quantum mechanical simulations of 10 nm InAs tri-gate quantum wire transistors. We have additionally presented a method for the inclusion of POP as a real-space self-energy term. We find that the ballistic performance of the devices can be recovered if the dopants in the system are kept away from the channel entrance and exit. When dopants are present at these key points, we find that the altered carrier energy, particularly in the source, has a significant impact on the device. This ballistic recovery is aided by the fact that at higher energies, POP scattering loses its non-locality which leads to a reduced scattering rate in these confined systems.

References

[1] H. S. Doyle, S. Datta, M. Doczy, S. Hareland, B. Jin, J. Kavalieros, T. Linton, A. Murthy, R. Rios, and R. Chau, IEEE Electron Dev. Lett. **24**, 263 (2003).

[2] R. Chau, S. Datta, M. Doczy, B. Doyle, B. Jin, J. Kavalieros, A. Majumdar, M. Metz, and M. Radosavljevic, IEEE Trans. Nanotech. **4**, 153 (2005).

[3] J.B. Boos, W. Krupps, D. Park, B. Molnar, and B.R. Bennett, Elect. Lett. **32**, 688 (1996).

[4] C.R. Bolognesi, E.J. Caine, and H. Kroemer, IEEE Elect. Dev. Lett. **15**, 16 (1994).

[5] M.J. Gilbert and D.K. Ferry, Superlatt. And Microstruct. **34**, 277 (2003).

[6] M.J. Gilbert and D.K. Ferry, J. Appl. Phys. **95**, 7954 (2004).

[7] J. Wang, E. Polizzi, and M. Lundstrom, J. Appl. Phys. **96**, 2192 (2004).

[8] D.D. Johnson, Phys. Rev. B **38**, 12807 (1988).

[9] M.J. Gilbert, R. Akis, and D.K. Ferry, J. Appl. Phys. **98**, 094303 (2005).